PNAS RESEARCH ARTICLE | ENGINEERING MEDICAL SCIENCES

Miniaturized, portable gustation interfaces for VR/AR/MR

Yiming Liu[a,b], Wooyoung Park[a], Chun Ki Yiu[a,c], Xingcan Huang[a], Shengxin Jia[a], Yao Chen[a], Hehua Zhang[a], Hongting Chen[b], Pengcheng Wu[a], Mengge Wu[a], Zhenyu Liu[a], Yuyu Gao[a], Kening Zhu[d], Zhao Zhao[e,f,1], Yuhang Li[g,h,i,j,1], Tomoyuki Yokota[b,k,1], Takao Someya[b,l,m,1], and Xinge Yu[a,c,n,1]

Affiliations are included on p. 11.

Edited by John Rogers, Northwestern University, Evanston, IL; received June 17, 2024; accepted October 16, 2024

Gustation is one of the five innate sensations for humans, distinguishing from vision, auditory, tactile, and olfaction, as which is a close and chemically induced sense. Despite the fact that a handful of gustation display technologies have been developed, the new technologies still pose significant challenges in miniaturization of the overall size for portability, enriching taste options within a limited working area, supporting natural human–device interaction, and achieving precisely controlled taste feedback. To address these issues, here, we report a set of intelligent and portable lollipop-shaped taste interfacing systems covering from 2 to 9 different taste options for establishing an adjustable taste platform in virtual reality (VR), augmented reality (AR), and mixed reality (MR) environments. Tasteful and food-grade chemicals embedded agarose hydrogels serve as taste sources based on iontophoresis operation principle, with an adjustable feedback intensity and independent operation time by tuning the voltage input. To achieve portability and user-friendly operation, the devices are miniaturized into a gustation interface with 9-channel taste generators in the dimension of 8 cm × 3 cm × 1 cm. To realize both gustation and olfaction feedbacks in Metaverse, an olfaction interface based on 7-channel odor generators is also introduced into the gustation interface system. As a result, the demonstrations of our gustation interface systems in intelligent medical gustation assessment, remote shopping, and mixed reality have proven their advances and great progress in various potential application areas, ranging from human–machine interfaces, to biomedical science, and to entertainment.

mixed reality | portable electronics | human machine interfaces | gustation interface | gustation assessment

Significance

Recent advances in virtual reality technologies (VR) have accelerated the foundation of flawless 3-dimension virtual worlds. Alongside visual, auditory, haptic, and olfactory sensations, taste significantly influences both the physiological and psychological aspects of human experience, however, the research in the development of taste-generating technologies in VR applications is still in its infancy. This study reports a concept of intelligent, portable lollipop-shaped gustation interfaces based on arrays of taste generators for gustatory VR applications. The miniaturized gustation interfaces support independent teleoperation for each channel of taste generators, providing adjustable taste intensity feedback. To demonstrate the advances of the gustation interfaces, three applications are designed, including medical gustation assessment, immersive remote shopping, and mixed reality applications.

Food intake, including eating and drinking, is one of the primary activities that humans engage in naturally since infancy to absorb essential nutrients for survival, during which the taste of food plays a crucial role in the gustation of satiation for promoting or suppressing appetite (1). Generally, human gustation consists of five basic flavors, including sweet, salty, sour, bitter, and umami, induced by chemical stimulation on the dorsum of the tongue and in parts of the larynx, pharynx, and epiglottis (2). As one of five typical human sensations, including vision, auditory, haptics, and olfaction, gustation allows us to avoid dangerous foods, and approach beneficial things by sensing these external stimuli, serving as a unique and efficient channel to communicate with surroundings (3). Gustation interface systems, as an intelligent taste generation technology, could supply specific information to users by generating target taste, exhibiting great potential in numerous applications, for instance, virtual, augmented, and mixed reality (VR/AR/MR), clinical treatment, entertainment, and education (4–6). Unlike the other four widely reported human sensory feedback technologies (7–24), to date, only very limited numbers of gustation interfaces have been developed based on several working principles, ranging from chemical, thermal, and electrical stimulations and iontophoresis (*SI Appendix*, Table S1).

Among these reported gustation interface systems, the chemical stimulation-based devices could display target tastes by applying flavoring chemicals directly onto the human tongue with the intensity determined by the quantity of chemicals (25). Nevertheless, the cumbersome size due to severe space requirement for chemical storage and the long delay time induced by the bulky mechanical liquid delivery system extensively limit the application areas. For temperature variations enabled gustation interface systems, the taste feeling could be stimulated by applying distinguished temperature distributions onto the human tongue (26). To achieve fast and accurate temperature manipulation, a high-power, heavy cooling subsystem, and additional temperature sensors are required, posing high challenges to system stability, biological safety, and simplification of control panels (26). Electrical stimulation, as the mainstream method adopted in gustation interface systems, is capable of displaying five basic flavors by

The authors declare no competing interest.

This article is a PNAS Direct Submission.

[1]To whom correspondence may be addressed. Email: zhaozhao@csei.org.cn, liyuhang@buaa.edu.cn, yokota@ntech.t.u-tokyo.ac.jp, someya@ee.t.u-tokyo.ac.jp, or xingeyu@cityu.edu.hk.

This article contains supporting information online at https://www.pnas.org/lookup/suppl/doi:10.1073/pnas.2412116121/-/DCSupplemental.

Published November 25, 2024.

controlling the frequency, intensity, and direction of electrical power into the human tongue (27–29). However, electrode patches positioned on or near the tongue will inevitably hinder intraoral activities, thereby degrading the eating experience (27). Moreover, observed differences in gustation between individuals may lead to stimulated taste biases (27). Iontophoresis has emerged as an alternative to overcome the aforementioned flaws, where iontophoresis utilizes the movement of ions through biosafe hydrogels to transport tasteful chemicals for realizing stable taste feedback at low electrical power (30). Although this method has exhibited exceptional advances over the conventional ones in terms of biosafety, power consumption, precise taste feedback, and more natural human–machine interaction, it still poses great challenges in the overall size for portability, supplying abundant taste options in a limited working area for achieving a broad taste variance, supporting user-friendly utilization in terms of operating procedures and instructions, and realizing intelligent system teleoperation. What's more, the hurdles existed significantly restrict the development of gustation interface in VR/AR and MR applications.

Here, we report a series of intelligent, portable lollipop-shaped gustation interfaces (LGIs), that consist of 2 to 9 different taste generators (TGs) based on iontophoresis, exploiting edible-grade, tasteful chemicals embedded agarose hydrogels, are developed, capable of producing adjustable taste sensations in virtual environments. By optimizing the layout of the electronics components on ultrathin flexible printed circuit boards (0.27 mm) and adopting a lightweight 3D printed Nylon lollipop exterior as the main body of the electronics, the gustation interface systems could realize a miniaturized overall size (8 cm × 3 cm × 1 cm) with a weight of 15.2 g @ 9-channel TGs, 12.36 g @ 5-channel TGs, and 11.5 g @ 2-channel TGs, which are convenient for users to utilize and carry around. Additionally, multiple integrated channels of TGs support independent or parallel operation by wirelessly manipulating the intelligent gustation interfaces according to the tasks in a virtual environment. The intensity of generated taste could be adjusted by variating the amplitude of voltage into each TG channel ranging from 0 V to 2 V, where 2 V is within the human body safe voltage range (0 to 30 V). And unlike the majority of reported works that require an external electrode to be mounted onto human skin around the mouth before operation, our gustation interfaces have no restrictions on the working conditions like a real lollipop as the current in each TG channel will not flow through human skin or tissue, further ensuring the users' safety. By monitoring the current flow and operation time in each TG channel, the gustation interfaces could accurately predict the generated taste mass and concentration based on self-developed data-driven mathematical models by communicating the data with the paired personal computer, distinguishing our intelligent gustation interface systems with reported ones. Considering the fact that extensive previous research works have demonstrated the strong correlation between olfactory sensation and the perception of food taste (31, 32), we also developed an olfaction/gustation combined interface (OGCI) system by integrating channels of miniaturized odor generators (OGs) into the gustation interface platform, which is rarely incorporated in reported gustation feedback system, capable of generating specific taste with corresponding odor released for extensively enhancing users' immersive experience in a virtual environment. As a result, benefitted from the user-friendly portability, well-designed device structure, high-channel taste generators, controllable tasteful solutions generation rate, and olfactory feedback system integrated, we have demonstrated the gustation interfaces family in three applications, including medical gustation assessment, immersive remote shopping, and MR with visual, audio, haptic, olfaction, and gustation sensations feedback.

Results

Schematic Illustrations and Operation Principle of the LGIs. Fig. 1*A* shows the concept of the gustation interfaces, extending the conventional VR/AR/MR technologies with visual, audio, and haptic feedbacks to one more dimension, gustation display, where users could experience the taste by directly licking the working area of the devices. Here, we developed three gustation interfaces with different numbers (2 to 9) of TG channels, allowing users to select the suitable one according to their preferences in various application scenarios. It is worth mentioning that since the working areas of the three LGIs remain consistent (~7.1 cm^2), more TG channels will result in a reduction in the volume of the tasteful agarose gel, as well as a decrease in the feedback intensity of each TG channel (*SI Appendix*, Figs. S11, S12). Fig. 1*B* shows the exploded view of the 9-channel gustation interface, composed of multiple layers stacked: i) a 3D printed Nylon skeleton (*SI Appendix*, Fig. S1) serving as the main body of the device with the sufficient structural strength to cope with any external unpredictable loads, meanwhile housing flavored agarose gels and a commercial lithium-ion battery (3.7 V, 100 mAh); ii) Edible-grade, agarose gels based, 9 channels of taste generators with different tasteful, food-grade chemicals embedded, including sugar, salt, citric acid, cherry, passion fruit, green tea, milk, durian, and grapefruit (Fig. 1 *C* and *D* and *SI Appendix*, Fig. S2; see details in *Characteristics*), here it is worth mentioning that the agarose gels will not melt in 35 °C water, which simulates the internal environment of the human oral cavity (*SI Appendix*, Fig. S3); iii) a control panel based on two layers of flexible printed circuit boards (FPCBs, thickness of 0.27 mm; Fig. 1*E* and *SI Appendix*, Fig. S4) with microcontroller (MCU), Bluetooth module, decoders, resistors, capacitors, N-type and P-type metal-oxide-semiconductor field-effect transistors (MOSFETs), and low dropout (LDO) linear regulators integrated, capable of wirelessly manipulating the number of operating TG channels and output voltage amplitude through self-developed Graphical User Interfaces (GUIs) in a virtual environment (Fig. 1 *A* and *E* and Movies S3 and S4).

To realize the iontophoresis effect of each TG channel, the current generated by the control panel will flow through the target flavored agarose gel for delivering the corresponding chemicals outsides; then users could enjoy the taste feedback by licking the working area of the LGI (Fig. 1*F*). When an electric field is generated between the ends of the gel, both electromigration, which is the directional migration of ions, and electroosmosis (33), which induces the flow of the solvent molecules in the gel regardless of the polarity (34, 35), are derived. For the reporting taste-generating system, as the mineral water is included in the gels, the surface of the tasteful agarose gel is unevenly charged. Therefore, the tasteful chemicals that combine with water molecules are exuded through electroosmosis by delivering the tasteful liquid to the whole surface area of the gel chaotically while a portion of tasteful solutions are collected in the cavity of the tasting side during the operation. Here, distinguished from the reported gustation display technologies, the current in each TG channel does not pass human skin or tissue, that allows the gustation interface to start working in advance, thereby achieving delay-free applications in VR/AR/MR environments. Fig. 1*G* and Movie S1 show that the simulated equivalent strains of the 3D printed Nylon-based back cover reach the yield strength of Nylon (48 MPa) in the external distributed pressure of 23.71 MPa. It proves the high stability of LGI against various external loads, because the normal operating pressure is

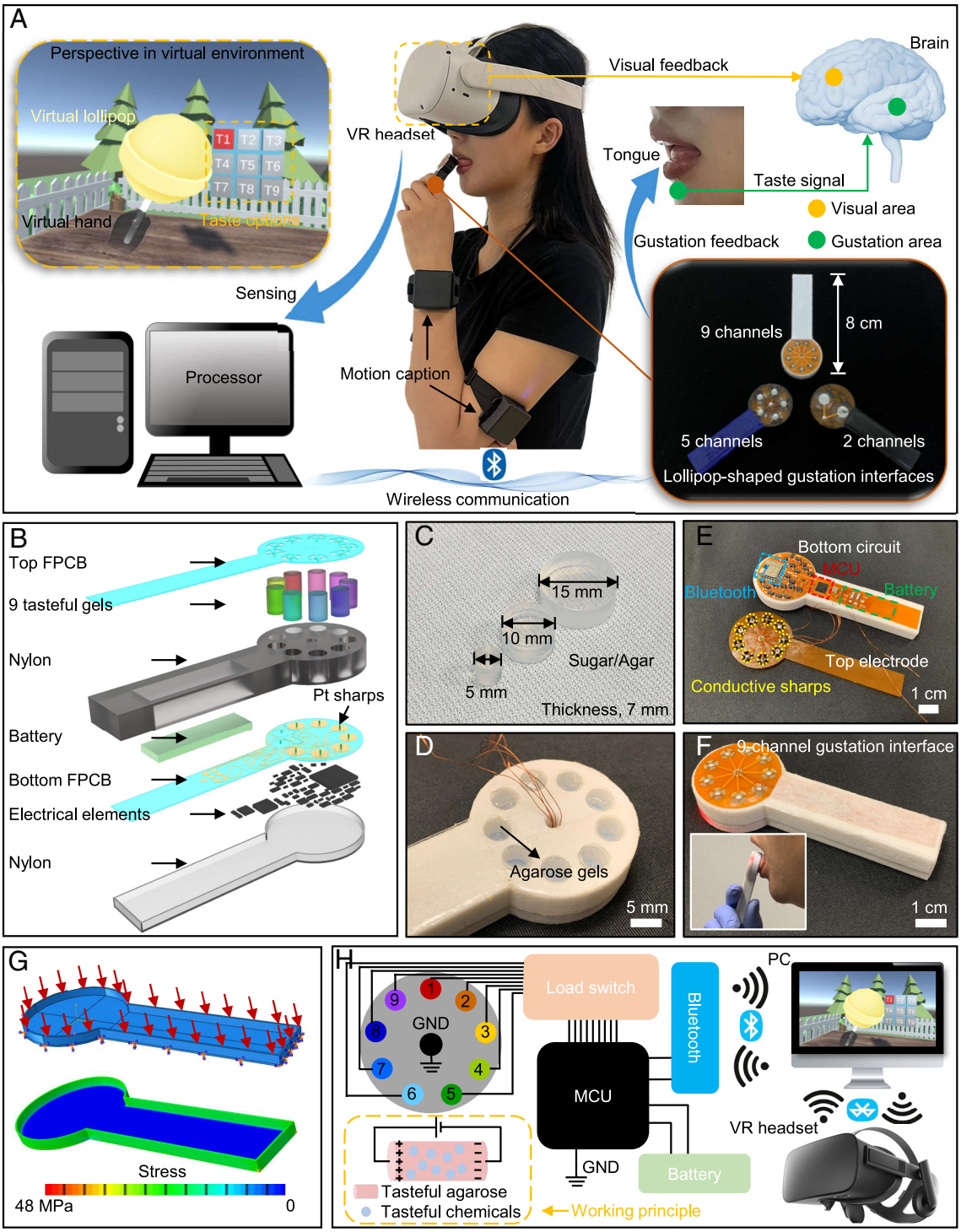

Fig. 1. Architecture and operation of the gustation interface systems. (*A*) Schematic diagram of the gustation interfaces for providing taste feedback to a female user in a virtual environment. (*B*) Exploded view of the 9-channel LGI with detailed descriptions on each layer. (*C*) Optical image of the adopted agarose-based gels with three diameters, 5 mm, 10 mm, and 15 mm. (*D*) Optical image of the working area of the 9-channel LGI. (*E*) Optical image of the two FPCBs used in the LGIs. (*F*) Optical image of a working LGI with an inserted subfigure showing the correct utilization method. (*G*) Mechanical stimulations of the 3D-printed Nylon back cover under the distributed external pressure. (*H*) Wireless operation process among the gustation interfaces, the VR glasses, and the PC.

much lower than the limit value obtained from FEA. The stress distributions of the 3D-printed Nylon back cover under various practical applications are presented in *SI Appendix*, Fig. S5. In *SI Appendix*, Fig. S5 *A* and *B*, the FEA results indicate that when subjected to uniformly distributed pressures on the handle root and the top arc, the maximum external stress could reach up to 1.13 MPa and 0.94 MPa, respectively. In *SI Appendix*, Fig. S5*C*, the FEA demonstrates the maximum uniformly distributed force that the upper surface of the back cover can withstand when users held at different handle positions (the entire, 2/3, and 1/3 of the handle). It is obvious that the maximum tolerable stress decreases with the decreasing gripping areas, 0.078 MPa @ the entire handle area, 0.077 MPa @ the 2/3 handle area, and 0.045 MPa @ the 1/3 handle area, and the calculated yield limits are sufficient during the practical applications. As a result, users could obtain the desired taste feedback by clicking the corresponding virtual button in a self-developed virtual environment to trigger the interfaced LGI (Fig. 1*H* and Movie S2), where the LGI installed with 9

different channels of taste is controlled by the separate 9 digital GPI/Os of a microcontroller unit (MCU) (ATMEGA328P-MU, Microchip Technology Inc.) in real-time, associated with external VR equipment (see more details in *SI Appendix*, Supplementary Note 1).

Movie S3 presents the wireless operation of the 9-channel gustation interface with each channel connecting a light-emitting diode (LED) in parallel for indicating the operating state, where we developed a simplified GUI for intuitive demonstration. Its excellent characteristics, stable operation, and fast response ensure a wide range of potential application areas for the LGIs, from human–machine interfaces, to medical treatment, and to Metaverse. To verify the anti-interference ability of the LGI during the practical application, the 9-channel LGI was programmed to alternately turn on /off two channels (sugar- and salt-based TG channels) at a constant frequency of 0.1 Hz with the working area sunk in deionized water (DI water) for simulating the environment in the human oral cavity, and the results have shown that the impact of water on the voltage output into each TG channel is negligible, demonstrating that users could accurately perceive the target taste without taste crosstalk (*SI Appendix*, Fig. S6). *SI Appendix*, Fig. S7 illustrates the stability test of the LGI, where the device is fully immersed in DI water with sugar-based TG channel operation for over 25 min at a frequency of 0.1 Hz, and the stable voltage output in the TG channel proves its good waterproof performance and long-term stability in complicated and harsh environment. To demonstrate the good potential of the LGIs in various practical applications, we measured the wireless communication distance of the 9-channel device in three different statuses, including standing freely, holding in the hand, and operating in the mouth, with the distance ranging from 9.4 m to 3.8 m, which meets the needs of various scenarios (*SI Appendix*, Fig. S8).

Electrical Characteristics of the 9-Channel TGs. Fig. 2 *A* and *B* show the generated chemical solution mass and pure chemical mass as a function of voltage amplitude into TG channels, tasteful chemical types, and operation time. Here, the voltage into each TG channel is set below 2 V for minimizing the potential safety issue in the complicated working environment (human mouth), as which may cause some unpredictable negative impact on the operation of LGIs in a long-term application. As observed in Fig. 2 *A* and *B*, along with the 1-h operation time, the 9 channel TGs could continuously exude tasteful solution with chemicals dissolved insides at a constant voltage input, for instance, from 3.6 mg solution with 1.9 mg at 1.5 min to 28.9 mg @ 5 mg at 60 min for sugar (2 V input), from 5.8 mg solution @ 1.3 mg at 1.5 min to 30.5 mg @ 4.9 mg at 60 min for passion fruit (1.5 V input), and from 5.9 mg @ 1.8 mg at 1.5 min to 35.3 mg @ 3.1 mg at 60 min for grapefruit (1 V input) (see more details in *SI Appendix*, Figs. S9 and S10), and it is also found that higher voltage into the 9 TG channels could contribute to a faster chemical generation rate, for example, from 2.4 mg with 1 V input to 3.6 mg with 2 V sugar solution at 1.5 min, from 43.6 mg citric acid solution @ 1.5 V to 48.9 mg @ 2 V at 36 min, and from 3.2 mg green tea chemical @ 1 V to 4.2 mg @ 2 V at 60 min, as higher voltages tend to increase the current flow within TGs, further accelerating the migration of charged water molecule (36). Here, we adopted the absorbent paper to collect the exuded chemical solutions by the TGs, then measured the mass variations of the solution-absorbed paper and the air-dried one for obtaining generated chemical solution mass and pure chemical mass, respectively.

To investigate the impact of the tasteful agarose gel's size on the electrical performance of TGs, we measured the mass of exuded chemicals and corresponding solutions as a function of agarose gel diameter from 5 mm to 15 mm, at a constant length and voltage input of 7 mm and 2 V, respectively (*SI Appendix*, Figs. S11 and S12). It is obvious that the tasteful gels with a larger size exhibit faster chemical and solution exudation rates, for example, from 1.9 mg with a gel diameter of 5 mm to 6.5 mg @ 15 mm durian solution at 6 min, from 3.3 mg @ 5 mm citric acid chemical to 5.2 mg @ 15 mm at 26 min, and from 3.4 mg @ 5 mm grapefruit chemical to 11.5 mg @ 15 mm at 36 min. Therefore, the 2-channel, 5-channel, and 9-channel LGIs (Fig. 1*A*) respectively adopt the gels with diameters of 5 mm, 10 mm, and 15 mm, resulting in a fact that the three devices own distinguished advantages and shortcomings over each other. For example, the 2-channel device could contribute the fastest chemicals exudation rate but provide minimum number of TG channels among the three LGIs. As a result, users could select the appropriate device according to their preferences. Fig. 2*C* and *SI Appendix*, Fig. S13 respectively show the normalized and absolute current into the 9 channel TGs as a function of operation time at a constant input voltage of 2 V, and it is found that both of the salt- and citric acid-based TGs exhibit distinguished current variation curves with those of the other 7-channel TGs, which may result from the abundant free ions in the two gels.

For the TGs based on salt and citric acid, during the chemical exudation process, the chemicals concentration in the gels increases along with the operation time except the extremely short period at the beginning (≤1.5 min), further decreasing the resistance of the gels due to the increasing free ions in gels (Fig. 2*D*). Here, the chemical mass percentage concentrations in Fig. 2*D* are calculated by dividing the mass of the pure chemicals by the total mass of the generated chemical solutions with the unit of wt%. Compared to the salt- and citric acid, the electrical conductivity of the embedded chemicals in the other 7-channel TGs is much poorer, leading to higher initial resistance (50 to 7,901 kΩ) of the gels (*SI Appendix*, Fig. S21). Therefore, the high chemical concentration exudation (>0.1, the initial chemicals concentration in gels) at the beginning state could contribute to lower chemicals concentration in the TG, resulting in a decreasing gel resistance and an increasing current flow through the gels. Following, the low concentration of the exuded chemicals (~0.1) and amount of water loss from each TG channels will inevitably reduce the electrical conductivity of the gels, causing current to continuously drop down, as observed in Fig. 2*D*. Here, the nonlinear chemical concentration variations may result from the difference between the loss rates of the pure tasteful chemicals and the gel base. Fig. 2 *E* and *F* respectively present the exuded chemical solution and pure chemical as a function of operation time in each TG channel at a constant voltage input of 2 V, and it is clear that all the TG channels tend to slow down the exudation rates of both chemical solution and pure chemical along with operation time, which may result from the continuous water loss in the gels. Therefore, 1 h as the full-load running lifetime for each TG channel is recommended for achieving optimal taste feedback experience. To monitor the taste generation rate and intensity in each TG channel, we developed two data-driven mathematical models based on operation time and corresponding current variations to respectively estimate the mass of chemical solution (total taste mass) and pure chemical (taste mass) in real time (Fig. 2 *G* and *H* and *SI Appendix*, Table S2). At the beginning state, the first 20-min operation time, the nonlinear fitted models indicate that the exudation process of both chemical solution and pure chemical may be majorly affected by the heating effects of electric current. Then, the exudation process was characterized as a linear relation with electric current as the exudation slowed down. The taste feedback could be precisely controlled by monitoring the exudation of

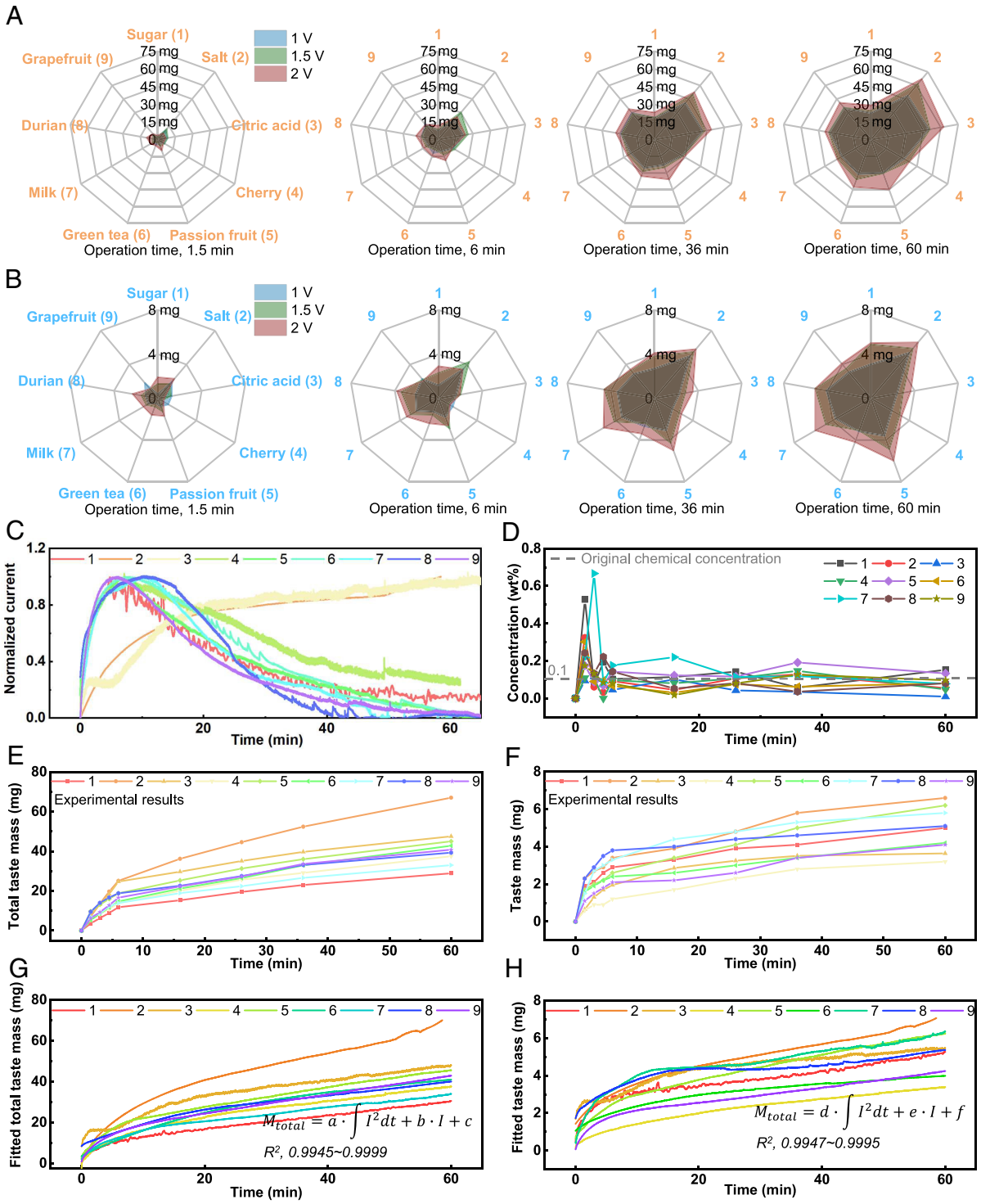

Fig. 2. Electrical performance of the taste interface with 9 channels. (*A*) The mass of the generated tasteful solution as a function of chemical types, operation time, and voltage input. (*B*) The mass of the embedded tasteful chemicals as a function of chemical types, operation time, and voltage input. (*C*) Normalized current flowing through 9 TG channels as a function of operation time. (*D*) Tasteful chemical concentration of 9 TG channels as a function of operation time. (*E*) The measured mass of the generated tasteful solutions by the 9 TG channels as a function of operation time. (*G*) The data-driven mathematical model fitted mass of the generated tasteful solutions by the 9 TG channels as a function of operation time. (*F*) The measured mass of the generated tasteful chemicals by the 9 TG channels as a function of operation time. (*H*) The data-driven mathematical model fitted (*H*) mass of the generated tasteful chemicals by the 9 TG channels as a function of operation time.

tasteful chemicals by inspecting the total operation time and corresponding current variations of each TG channel. *SI Appendix*, Fig. S14 shows the total mass loss of the 9 tasteful gels with the 9 different chemicals embedded under the three different testing conditions: 1) the first one is an open-air environment of 21 °C; 2) the second one is a practical application where one user enjoys the LGI based on his own eating habits; 3) the third one is that all gels were operated in 35 °C DI water. It is interesting to find that the average total mass loss of the gels in the second testing condition (operation in user's mouth) is the highest, which may be induced by the frequently sucking the LGI during the application. As a result, we think many unpredictable parameters may have potential effects on the chemical generation mass of the LGI, including users' eating habits, ambient temperature, and humidity.

Biosafety and Stability of the Taste Generators. In order to verify the consistency of the properties of chemicals before and after exudation through iontophoresis, we respectively measured the Raman spectrum of TGs exuded sugar and citric acid solutions in the spectral regions 1,000 to 1,500 cm^{-1} and 400 to 1,800 cm^{-1} (Fig. 3 *A* and *B*). The principal bands of the spectrum can be assigned to several vibrational modes of the sucrose molecule and keep consistent with that of the sucrose that have been published previously (37, 38). Similarly, the spectrum bands of the TGs exuded citric acid electrolyte are consistent with the characteristic of citric acid (39). As a result, the Raman spectrum proves that the iontophoresis would not change the electrolyte contents and induce other substances. Furthermore, we test the exudation time of the iontophoresis using our previously reported state-of-the-art sodium ion (Na^+) sensor (40). As shown in Fig. 3*C*, the Na^+ concentration on the agarose surface would remain a constant value due to the sodium chloride (NaCl) electrolyte in the agarose. When the voltage is applied on the agarose, the output of Na^+ sensor would increase within about 0.27 s, indicating the increase of Na^+ concentration and rapid reaction time of the TG. Further, we adopted the Na^+ sensor to monitor the Na^+ concentration generated by the TG channel every 1.5 min with the result (*SI Appendix*, Fig. S15) approaching to that in Fig. 2*D*, proving the fact that the chemical concentrations by the TGs will increase

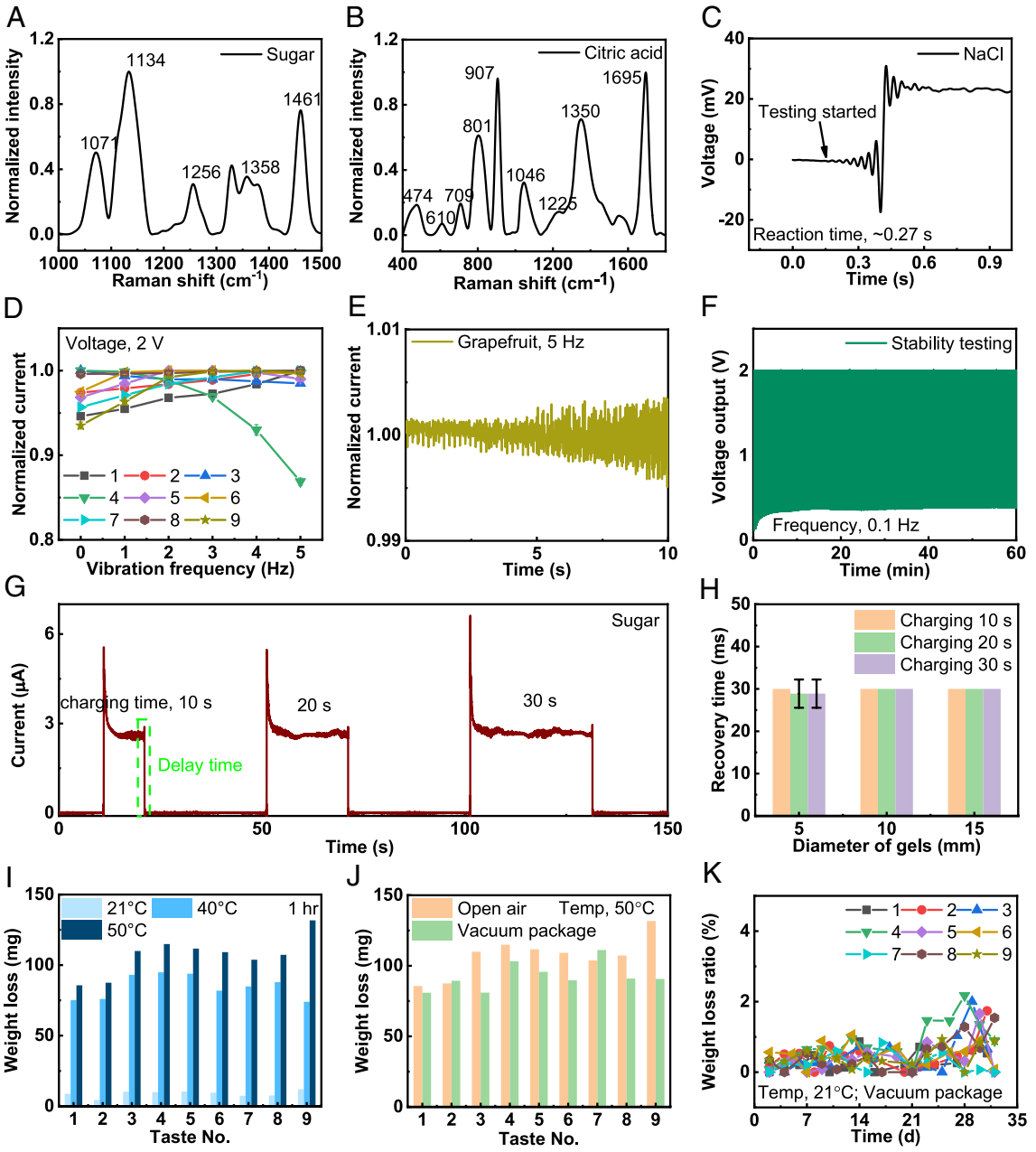

Fig. 3. Biosafety and stability of the TGs. (*A* and *B*) Raman spectra of the exuded solutions by the sugar (*A*) and citric acid (*B*) based TG channels. (*C*) Electrical response of a NaCl sensor to the solution generated by the NaCl embedded TG channel. (*D*) Normalized current of the 9 TG channels as a function of the vibration frequency ranging from 0 to 5 Hz with a constant voltage input of 2 V when the LGI is fixed onto a commercial oscillator. (*E*) Normalized current of the grapefruit-based TG channel as a function of operation time at the vibration frequency of 5 Hz. (*F*) Voltage signal between the cherry-based TG channel as a function of operation time at the voltage input amplitude and frequency of 2 V and 0.1 Hz, respectively. (*G*) Current signal of the sugar-based TG channel at a voltage input of 2 V as a function of operation time with the three different charging times ranging from 10 s to 30 s. (*H*) Average recovery time of all agarose gels with three different sizes and 9 different tasteful chemicals embedded. (*I*) Weight loss of the 9 TGs after exposed in air for 1 h at the three different ambient temperature (21 °C, 40 °C, and 50 °C). (*J*) Weight loss of the 9 TGs with the two storage methods (vacuum package and open air) at the ambient temperature of 50 °C. (*K*) Long-term weight loss monitoring of the 9 TGs stored in vacuum packaging at an ambient temperature of 21 °C.

to the peak values within a few minutes (≤3 min), then drop to a stable level till the end. *SI Appendix*, Fig. S18 further proves the exuded sugar chemical by testing the reaction of the glucose test papers with and without sucrose invertase treated. Besides the NaCl embedded TG, we also measured the reaction time of the citric acid–based TG by adopting the self-developed pH sensor (41) with the value of 0.1 s, as shown in *SI Appendix*, Fig. S16. In addition to the tests shown in Fig. 3 *A*–*C* and *SI Appendix*, Fig. S16, we also conducted a series of volunteer tests to further investigate the consistency of the 9 tasteful chemicals (sugar, salt, citric acid, cherry, passion fruit, green tea, milk, durian, and grapefruit) before and after exudation through iontophoresis, as shown in Fig. 4, which will be described in details later. Here, the reaction time is defined as the time which the biosensors require to detect the target chemicals generated by the TGs. As a result, it is found that the 9 embedded chemicals could be exuded with their original chemical characteristics through the iontophoresis, ensuring the biosafe application of the LGIs to users. To demonstrate the stability of the 9-channel gustation interface system, the LGI was fixed onto a programmable commercial oscillator with controllable vibration frequency during full-load operation of the LGI (voltage input, 2 V), then the vibration frequency variates from 0 to 5 Hz at an interval of 1 Hz with a vibration amplitude of 1.86 mm (Fig. 3 *D* and *E*). It is obvious that all TG channels kept stable with negligible fluctuations at the vibration frequency ≤4, where the normalized current values in each channel range from 0.93 to 1. The low current fluctuations demonstrate the high stability and accurate control in exuding tasteful chemicals of the LGI as interfaced with human beings in daily life, where it is reported that the frequency range of human daily activities was shown to be between 0.3 and 3.5 Hz (42). Fig. 3*F* and *SI Appendix*, Fig. S19 show the stability test of the LGI by inputting a constant voltage (2 V) into the cherry-based TG channel at a frequency of 0.1 Hz, and 60-min stable operation proves the good stability of the device. It is worth mentioning that the voltage between the TG channel requires 5 s to drop from 2 V to 0.35 V when the power into the TG is shut down, which may result from a fact that the agarose gel and two-side electrodes function as a capacitor to store electrical energy during operation and release it when power is off. To investigate the capacitor effect on the electrical performance of the TGs, we measured the current response of the gels with different overall sizes (diameters, 5 mm, 10 mm, and 15 mm; thickness, 7 mm) in the 9 TG channels when operating time (also called charging time for capacitors) variating from 10 s to 30 s (Fig. 3 *G* and *H* and *SI Appendix*, Fig. S20), and it is interesting that the delay time (time it takes for the current to drop to 0 when the power into each TG is cut off) of all TG channels keeps around 30 ms, thereafter, the voltage in the TG channel leaks slowly after turning off the power input, as shown in *SI Appendix*, Fig. S19. Besides, the 30 ms delay time further demonstrates the excellent electrical performance of the LGIs, ensuring the smooth user experience in virtual environments.

Fig. 3 *I* and *J* show the impacts of ambient temperature (21 °C, 40 °C, and 50 °C) and tasteful gels storage methods (open air and vacuum package) on the weight loss of gels, and it is obvious that higher ambient temperature and open-air storage will accelerate the weight loss of gels, inevitably resulting in chemicals exudation later by iontophoresis. Therefore, to ensure the effectiveness of the taste gels during the application, all prefabricated gels are vacuum-packed and then stored at room temperature (~21 °C) before assembling them into the LGIs for operation. Fig. 3*K* shows the weight loss of the 9 different tasteful gels (channel numbers correspond to those shown in Fig. 2) as a function of vacuum package time over 30 d, and it is found that the average weight loss of the gels rises slowly from 0.2% at 2nd day to 0.9% at 30th day, further demonstrating the potentials for future commercialization and outdoor long-term applications. *SI Appendix*, Fig. S21 presents the initial resistance of the 9 tasteful gels with the results shown as the following: 7.9 MΩ @ sugar, 11.7 kΩ @ salt, 9.3 kΩ @ citric acid, 135.5 kΩ @ cherry, 67.1 kΩ @ passion fruit, 60.5 kΩ @ green tea, 60 kΩ @ milk, 50.1 kΩ @ durian, and 69.8 kΩ @ grapefruit. At a constant voltage input in each TG channel, higher resistance of the gels results in a lower current flowing through, inducing a lower mass of exuded chemicals (*SI Appendix*, Fig. S13 and Fig. 2 *E* and *F*). *SI Appendix*, Fig. S22 shows the pH values of the 9 gels ranging from 1 to 7, and it is worth mentioning that due to the limited amount of exuded citric acid (*SI Appendix*, Figs. S11 and S12), the generated citric acid (pH, 1) will be diluted by saliva to a safe level (over 2) before swallowing, making it biosafe for users. *SI Appendix*, Fig. S17 shows a volunteer test to demonstrate the similarity between the generated chemical solutions by the TGs and the original chemical solutions, where we define a range of similarity scores from 0 to 3, corresponding to the zero similarity and 100% identity. It can be seen that the 7 volunteers' average score is 2.14, indicating that these volunteers could accurately identify the type of generated chemicals.

Development of Olfaction and Gustation Combined Feedback Systems. Benefitted from the suitable working and well-designed concept, the family of miniaturized, intelligent lollipop-shaped gustation interfaces have been developed in various potential application areas, ranging from entertainment, to medical instrumentation, and to education. To further enrich the immersive experience to users in virtual environments, we integrated a detachable olfaction interface module with 7 OGs onto the backside of the 9-channel LGI platform, as shown in Fig. 4*A*, where the OGs can be programmed to release or terminate the target odor by manipulating the current direction flowing through the copper (Cu) coils (*SI Appendix*, Figs. S24 and S25). Here, we adopted 4 V as the constant voltage into each Cu coil due to the limited inner height of the OGs chamber (*SI Appendix*, Fig. S26), and 4 V is also the minimum voltage required for lifting the magnet up due to weight of the magnet (diameter, 6 mm; thickness, 0.5 mm) and the attached bending platform (thickness, 1 mm). *SI Appendix*, Fig. S27 shows the stability test of the OG by continuously switching the voltage input direction at a frequency of 1 Hz for over 5,400 cycles, and the stable operation of the OG demonstrates the good potentials of the OGCI in practical applications. See the detailed structural difference between the 9-channel LGI and the OGCI in *SI Appendix*, Supplementary Note 2 and Fig. 4*B*. Due to the olfaction interface module, the OGCI shares a same lollipop-shape size with the LGIs but owns a thicker height (1.25 cm and 1 cm for OGCI and LGIs, respectively), as shown in Fig. 4*C*.

To further demonstrate the advances of the OGCI over the LGIs, we conducted a series of volunteer tests in evaluating volunteers' recognition rates and corresponding response time of the 9 different tastes with the data automatically collected by a self-developed GUI (Movie S3), where 20 volunteers (8 males and 12 females) are evenly divided into two testing groups: one group (4 males and 6 females) for experiencing pure taste feedback though the 9-channel LGI, and the other one group for both odor and taste feedbacks though the OGCI (Fig. 4 *D*–*K*). During the test, the paired PC will command the LGI (or OGCI) to randomly generate a specific taste (and the corresponding odor for OGCI) to volunteers, then the volunteers could give their answer by clicking the button on the GUI for data collection. Once the answer is recorded by the PC, a new command will be sent to the LGI (or OGCI) after 1 min until all the 9 tastes are generated. Here, the

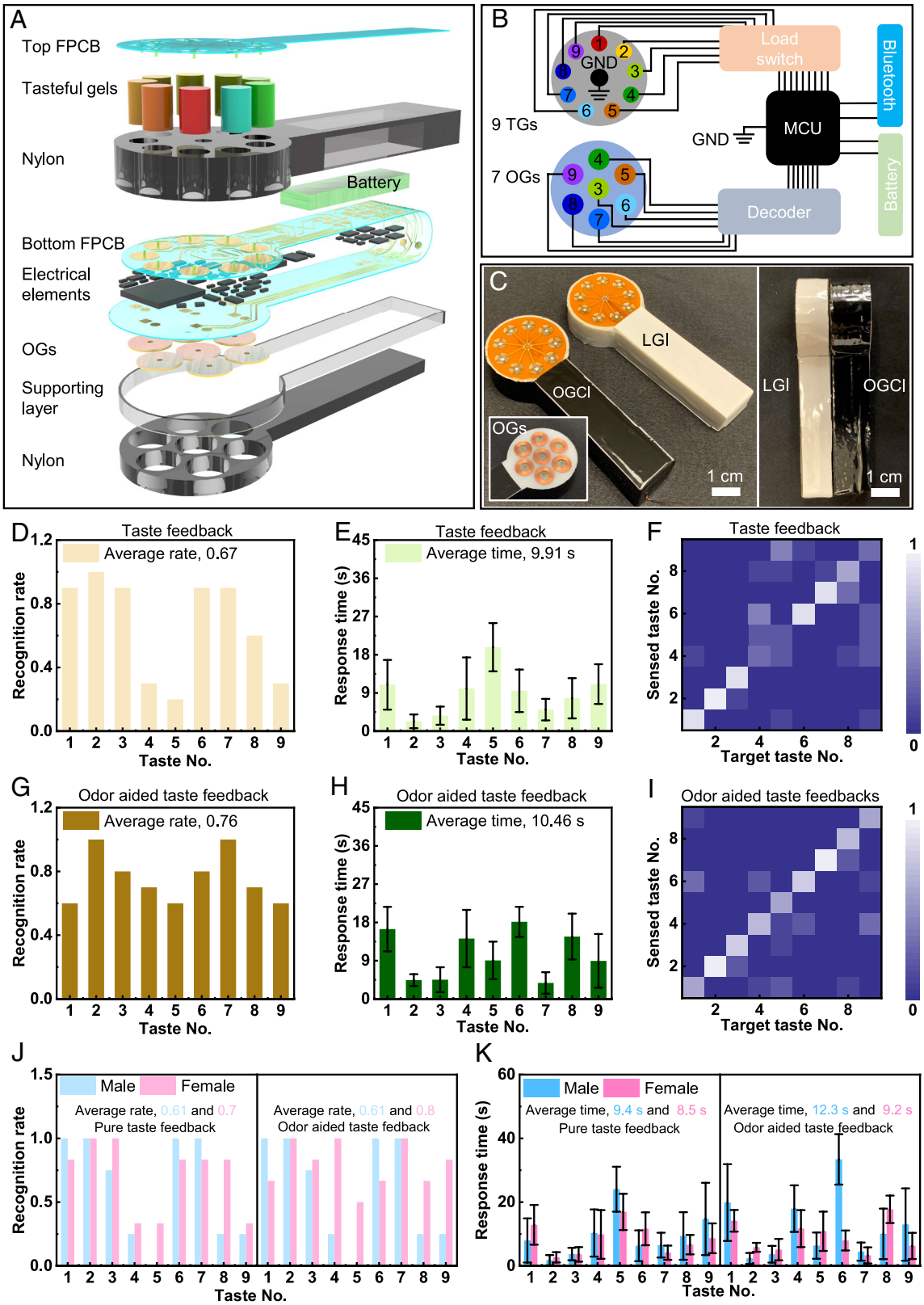

Fig. 4. Structure of the OGCI and the corresponding volunteer testing results. (*A*) Exploded view of the OGCI with the detailed description for each component. (*B*) Circuit design of the OGCI. (*C*) Optical images of the 9-channel LGI and the OGCI. (*D* and *G*) Recognition rate of 10 volunteers in recognizing 9 different tastes by respectively using the 9-channel LGI (*D*) and OGCI (*G*). (*E* and *H*) Response time of 10 volunteers in reacting 9 different tastes generated by respectively using the 9-channel LGI (*E*) and OGCI (*H*). (*F* and *I*) Training confusion results as a function of taste channel number of the 9-channel LGI (*F*) and OGCI (*I*). (*J* and *K*) Recognition rate (*J*) and response time (*K*) of the volunteers from the two testing groups (pure taste feedback by the LGI and the odor/taste feedbacks by OGCI) as a function of gender.

1-min interval is to avoid the odors crosstalk due to the measured odor recovery time shown in *SI Appendix*, Fig. S28. As observed in Fig. 4 *D*–*I*, odor-aided taste feedback system realized by the OGCI could achieve a higher average recognition rate (0.76) than that (0.67) of the pure taste feedback (the 9-channel LGI), but the average response time is slightly longer (10.46 s @ OGCI, and

9.91 s @ LGI), which may be due to the fact that people could obtain more external information from taste and olfactory feedbacks than that only from taste channels before making a final decision. Here, the response time is defined as the time which users need to physiologically sense the tasteful chemicals generated by the gustation interface systems.

In addition, it is also interesting to find that the female volunteers exhibit a better gustation capability with higher recognition rates and lower response time over that of the male ones in both two testing groups, as shown in Fig. 4 *J* and *K*. As a result, compared to the LGI, the OGCI could contribute a richer immersive experience to users but owns a larger overall size and higher weight, so users could select a suitable device according to their preferences in various application areas. *SI Appendix*, Fig. S29 shows the operation time of the three LGIs and OGCI at a full load with the time ranging from 0.94 h to 4.3 h, where a full load demonstrates that we turn on all working TG and OG channels with the wireless communication between the device and the paired PC. By balancing the overall size of the electronics and operation time, the OGCI adopts the 300-mAh battery (41 mm × 13 mm × 5 mm) with the full-load operation time of 0.94 h, which could cover the needs of the most application scenarios as the adopted tasteful gels are recommended to be replaced after 1-hr operation as mentioned before.

Demonstrations of the Gustation Interface Systems. In Fig. 5, three different demonstrations for the gustation interface systems showcase their advances in building up an intelligent, unique taste feedback platform. One of the application areas for the gustation interfaces is to conveniently conduct a comprehensive and objective gustation test for users (Fig. 5*A*). Gustatory disorders are classified clinically as either quantitative or qualitative (43). To date, there is a lack of standardization for gustatory testing and no universally accepted method. There are also no clinically useful objective tests of gustation (44, 45), and majorly rely on subjective tests. One of the conventional gustation evaluation methods involves the subjects' taste thresholds measurement in sour, sweet, bitter, salty, and umami. During the evaluation, testers prepare a series of concentrations of solutions containing one of the five basic tastes, then provide the solutions to the subjects in the order of increasing concentration, where the lowest concentration the subjects could recognize is the threshold value for the corresponding taste type (Fig. 5 *A*, *i*). However, the time-consuming solutions preparation, large result errors, and inefficient testing operations pose a difficult task for both of the clinician and subjects to conduct the gustation test. To solve this issue, our 9-channel LGI could be adopted for assessing subjects' gustation capability in a short time with results synchronously displayed on screen for later data analysis (Fig. 5 *A*, *i*), where the 6 volunteers are required to lick the working area of the LGI with a random taste generated until giving the answer on the taste type by clicking the corresponding button in a self-developed GUI (same as that in Movie S2). Here, apart from the subject's taste recognition rate, we also took the corresponding consumed time into consideration since the operation time of TG could also indicate the tasteful chemical concentration at which the subject identifies a taste. According to the results shown in Fig. 2*D*, the chemicals concentration of the generated 9 different TG channels will continuously increase to the peak values in the first 3 min, during which longer response time demonstrates a higher threshold value for the corresponding taste types, resulting in a lower response time score for assessing users' gustation capability. It is worth mentioning that all the 9 different taste chemicals were used during the volunteer test for comprehensively evaluating users' gustation. Benefitted from the user-friendly operation for the users, the 6 volunteers could finish the test in a short time (40.2 s to 119.8 s). As a result, the visualization of the gustation test results is also shown through polygon charts with empirical score to evaluate the volunteers' gustation capability, as shown in Fig. 5 *A*, *ii*. Following our previous work (46) that employed a list-wise recommendation framework, the score was defined as a weighted sum of the evaluation of recognition time and the scaled response time between the minimum and maximum values.

Then, an immersive online shopping was realized by exploiting the gustation interface system associated with VR headsets, supporting the visual, audio, and gustation feedbacks (Fig. 5*B*). In this application, users can select a specific taste option by touching the corresponding virtual food in a virtual grocery with a 9-channel LGI realizing the taste feedback. Here, once the target food is selected, the taste generation of the corresponding LGI channel is instantly activated by switching up the iontophoresis between the two ends of the tasteful agarose gel (voltage input, 2 V). Following, in one experiment, three different taste channels were examined, including passion fruit, green tea, and grapefruit, where, according to the user's selection, each channel could be turned on and off consecutively with the corresponding electrical current flows displayed for further verifying the generation of different flavors (Fig. 5*B*). Here, the working time of the three TG channels ranges from 24 s to 36 s, which is sufficient for users to perceive the taste feedback (Fig. 4*E*).

A MR-based immersive virtual system is developed with all the five basic senses of humans, including gustation, olfaction, haptic, audio, and vision, based on the combination of a VR headset and OGCI, where, for example, children could conveniently learn the characteristics and features of various food in a short time under the supervision of their parents (Fig. 5 *C*, *i* and *ii* and *SI Appendix*, Supplementary Note 7). In this MR system, visual and audio feedbacks are provided by the VR headset, olfaction and gustation display is realized by our OGCI, and the haptics is achieved by the real lollipop device, where users could directly hold the device during the MR application. During the application, the OGCI and the corresponding virtual model share the same 3D position coordination in both of reality and virtuality. In the VR scenario, nine different virtual buttons, marking names of specific taste and olfaction channels, are built in for controlling the OGCI in generating particular flavors and odors (Fig. 5 *C*, *iii*). During the utilization, once a virtual button is selected by virtual touch realized by the hand tracking system and the lollipop is held by the user, commands for manipulating the intelligent OGCI system are transmitted wirelessly to activate corresponding taste and olfaction channels (Fig. 5 *C*, *iii* and Movie S4), where, in the experiment, taste, and olfaction channels for sugar, cherry, milk, and grapefruit were opened consecutively according to the commands received from the VR equipment. During the experiment, the taste channel was activated for a brief period of 10 s. However, according to the average recognition time shown in Fig. 4*E*, this 10 s activation should be sufficient to meet the 9.91 s average recognition time for different tastes. Additionally, the activation time can be adjusted according to the specific taste and user preferences. As a result, the three typical demonstrations shown in Fig. 5 have proven the great potentials of our gustation interface family in wide application areas, ranging from human–machine interfaces, to medical evaluation, to education, and to entertainment. In addition to the LGIs and OGCI, we also developed a 9-channel LGI with a thermistor integrated for minimizing the temperature effect on chemicals generation mass prediction, as shown in *SI Appendix*, Figs. S30 and S31. The thermistor, mounted at the bottom of the LGI working surface, could accurately monitor the temperature near the TG channels, therefore,

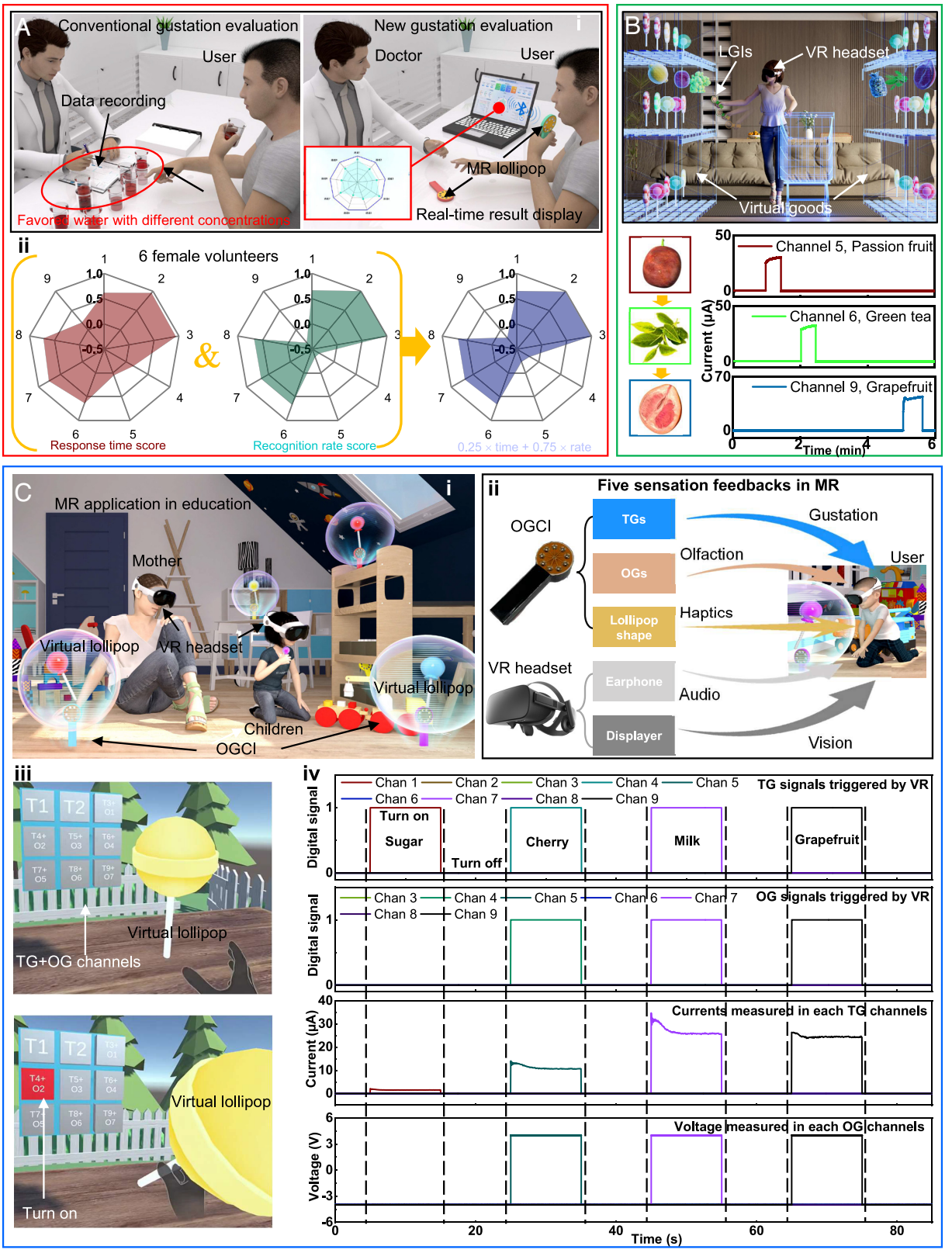

Fig. 5. Three typical demonstrations of the gustation interfaces. (*A*) A demonstration of the 9-channel LGI in providing an alternative gustation evaluation method (*A–i*) with the assessed test result of 6 female volunteers shown in *A–ii*. The 9 tasteful gels follow the setting of Fig. 2*A*. Negative scores are assigned to false detection while positive values indicate correct identification. (*B*) A demonstration of the 9-channel LGI in displaying the taste feedback to a female user in a virtual online shopping scenario for providing an immersive experience (*B–i*), and the three TG channels (passion fruit, green tea, and grapefruit) were turn on one by one, where the corresponding operating time is consistent with the user's motion in the virtual environment (*B–ii*). (*C*) A demonstration of the OGCI in providing odor and taste feedbacks to users in a MR-based educational application (*C–i*), where a mother is teaching her son the tastes and odors of some fruity lollipop. Here, due to the characteristics of the MR, users could experience five basic sensation feedbacks, including gustation/olfaction/haptic feedbacks @ OGCI, and vision/audio feedbacks @ VR glasses (*C–ii*). In a practical MR application, a user experienced the four different tastes (sugar, cherry, milk and grapefruit) and corresponding odors by utilizing the OGCI in a virtual environment (*C–iii*), during which taste and olfaction channels for sugar, cherry, milk, and grapefruit were opened consecutively according to the commands received from the VR equipment (*C–iv*).

once the detected temperature exceeds the preset value (for example, 28 °C), the prediction of the chemical generation will be paused by stopping the current measurement in all TG channels, where the preset value is used to distinguish whether the LGI is in the mouth or not. *SI Appendix*, Fig. S32 presents the detected temperature variations as a function of operation time, during which the new LGI was repeatedly soaked into 34 °C water for four cycles, and it is obvious that the device could rapidly response to the surrounding temperature variations. To further demonstrate the LGI in practical applications, a user was required to repeatedly lick and take away the LGI, meanwhile the device continuously monitored the electrical signal of the thermistor with the current measured intermittently, as shown in *SI Appendix*, Fig. S33. However, considering some unpredictable parameters effect (for example, surrounding humidity and users' eating habits), our gustation interfaces family may fail to provide an accurate prediction of the chemical generation rate and mass. We hope to provide a reliable solution to measure the chemicals release directly in the future.

Conclusion

In summary, we developed a series of intelligent, portable gustation interface systems in the format of the lollipop, supporting both of taste and olfaction feedbacks in virtual environments. Based on iontophoresis working principle, our LGIs and OGCI could be programmed to separately manipulate the exudation intensity and time of tasteful chemicals embedded in agarose gels in the nine TG channels with a small working area of 7.1 cm^2, realizing a miniaturized structure design for the user-friendly utilization. Besides, the gustation interfaces enable the real-time recording of taste generation rate and exudation chemical mass based on the current and operation time for each TG channel by integrating a data-driven mathematic model. By designing the three different demonstrations, including clinical gustation evaluation, immersive online shopping, and educational MR experience with five basic sensation feedbacks, our gustation display family has demonstrated their advances over the reported works in electrical performance (response time, stability, and anti-interference), overall size, the number of TG channels, the combination of olfaction feedback, intelligence during operation, and potential application fields, further proving their significant potentials in human–machine interfaces, education, entertainment, and medical diagnosis. However, the current gustation interfaces fail to realize a controllable chemical concentration in exuded solutions, which will be solved in the future by trying different working principles.

Methods

Fabrication of Tasteful Gel. To fabricate the tasteful gels, 0.6 g agarose is added into 20 mL mineral water stored in a 100-mL beaker, and then the mixture solution is melted in a microwave oven for 1 min. Following, 2 g target flavoring essence (including sugar, salt, citric acid, cherry, milk, green tea, passion fruit, durian, and grapefruit) is added into the melt agarose-based gels. Mix the sample on the magnetic stirrer at the heating temperature and spinning speed of 80 °C and 200 rpm for 1 min, then cure the gel in the room temperature for 10 min. Finally, cut the gels into the target size by a customized round cutter. Purchasing information for all chemicals adopted is listed in *SI Appendix*, Supplementary Note 3.

Fabrication of the LGIs and OGCI. Two flexible circuits were developed by adopting flexible printed circuit board (FPCB) techniques with a copper conductive layer plated with gold. All components, including a Bluetooth module, microcontroller, resistors, capacitors, etc., were soldered to the FPCBs. Finally, the circuits were mounted onto a 3D-printed Nylon skeleton, with the top and bottom FPCBs secured and decorated with colorful stickers. Detailed fabrication processes of the LGIs and OGCI can be found in *SI Appendix*, Supplementary Notes 4 and 5, respectively. In addition, the operation of the circuits in LGIs and OGCI could be found in *SI Appendix*, Supplementary Note 6.

Mechanical Simulation. The FEA commercial software ABAQUS (Analysis User's Manual 2020) was used to obtain the stress distribution of LGI under the distributed external pressure. Please find more details in *SI Appendix*, Supplementary Note 8.

Data, Materials, and Software Availability. All study data are included in the article and/or supporting information.

ACKNOWLEDGMENTS. This work was supported by National Natural Science Foundation of China (Grant No. 62122002), City University of Hong Kong (Grant Nos. 9667221, 9680322, and 9678274), Research Grants Council of the Hong Kong Special Administrative Region (Grant Nos. RFS2324-1S03, 11213721, 11215722, and 11211523), in part by Innovation Hong Kong Project on Project 2.2–AI-based 3D ultrasound imaging algorithm at Hong Kong Centre for Cerebro-CardiovascularHealth Engineering, Shenzhen Science and Technology Innovation Commission (Grant No. SGDX20220530111401011), the National Natural Science Foundation of China (Grant Nos. U23A20111 and 12372160), 111 Center (Grant No. B18002), Japan Society for the Promotion of Science (Grant No. 22K21343), and State Administration for Market Regulation Science and Technology Plan Project (Grant No. 2023MK201). This work was also supported by the Japan Society for the Promotion of Science (JSPS) Postdoctoral Fellowships for Research in Japan and JSPS Grants-in-Aid for Scientific Research (KAKENHI) Grant Number 24KF0025.

Author affiliations: [a]Department of Biomedical Engineering, City University of Hong Kong, Kowloong Tong, Hong Kong; [b]Department of Electrical Engineering and Information Systems, The University of Tokyo, Tokyo 113-8656, Japan; [c]Hong Kong Center for Cerebra-Cardiovascular Health Engineering, Hong Kong Science Park, New Territories 999077, Hong Kong; [d]Department of Computer Science, City University of Hong Kong, Kowloong Tong, Hong Kong; [e]China Special Equipment Inspection and Research Institute, Beijing 100029, China; [f]Technology Innovation Center of Health Management of Large-scale Amusement Device, State Administration for Market Regulation, Beijing 100029, China; [g]Institute of Solid Mechanics, Beihang University, Beijing 100191, China; [h]Tianmushan Laboratory, Hangzhou 311115, China; [i]Liaoning Academy of Materials, Shenyang 110167, China; [j]Aircraft and Propulsion Laboratory, Ningbo Institute of Technology, Beihang University, Ningbo 315100, China; [k]Institution of Engineering Innovation, The University of Tokyo, Tokyo 113-8656, Japan; [l]Institute of Physical and Chemical Research Center for Emergent Matter Science, Saitama 351-0198, Japan; [m]Thin-Film Device Laboratory, RIKEN, Saitama 351-0198, Japan; and [n]Institute of Digital Medicine, City University of Hong Kong, Kowloon, Hong Kong

Author contributions: Y. Liu, T.S., and X.Y. designed research; Y. Liu, W.P., C.K.Y., X.H., Y.C., H.Z., P.W., M.W., Z.L., and Z.Z. performed research; Y. Liu contributed new reagents/analytic tools; Y. Liu, W.P., S.J., H.C., and Y.G. analyzed data; and Y. Liu, W.P., C.K.Y., X.H., S.J., K.Z., Y. Li, T.Y., T.S., and X.Y. wrote the paper.

1. L. Cifuentes, A. Acosta, Homeostatic regulation of food intake. *Clin. Res. Hepatol. Gastroenterol.* **46**, 101794 (2022).
2. R. L. Doty, Gustation. *Wiley Interdiscip. Rev. Cogn. Sci.* **3**, 29–46 (2012).
3. L. A. Barlow, Progress and renewal in gustation: New insights into taste bud development. *Development* **142**, 3620–3629 (2015).
4. M. Ohno *et al.*, Anodal electrical stimulation enhances the perceived piquancy induced by chili peppers and wasabi. *IEEE Access* **10**, 134647–134654 (2022).
5. X. Yu *et al.*, Skin-integrated wireless haptic interfaces for virtual and augmented reality. *Nature* **575**, 473–479 (2019).
6. Z. Sun, M. Zhu, X. Shan, C. Lee, Augmented tactile-perception and haptic-feedback rings as human-machine interfaces aiming for immersive interactions. *Nat. Commun.* **13**, 5224 (2022).
7. J. Lee, D. Kim, H. Sul, S. H. Ko, Thermo-haptic materials and devices for wearable virtual and augmented reality. *Adv. Funct. Mater.* **31**, 2007376 (2021).
8. M. Zhu *et al.*, Haptic-feedback smart glove as a creative human-machine interface (HMI) for virtual/augmented reality applications. *Sci. Adv.* **6**, eaaz8693 (2020).
9. K. Nan *et al.*, Compliant and stretchable thermoelectric coils for energy harvesting in miniature flexible devices. *Sci. Adv.* **4**, eaau5849 (2018).
10. A. Stier *et al.*, Stretchable tattoo-like heater with on-site temperature feedback control. *Micromachines* **9**, 170 (2018).
11. S. Hong *et al.*, Wearable thermoelectrics for personalized thermoregulation. *Sci. Adv.* **5**, eaaw0536 (2019).
12. W. Heng, S. Solomon, W. Gao, Flexible electronics and devices as human–machine interfaces for medical robotics. *Adv. Mater.* **34**, 2107902 (2022).
13. T. H. Kim *et al.*, Printable, flexible, and stretchable forms of ultrananocrystalline diamond with applications in thermal management. *Adv. Mater.* **20**, 2171–2176 (2008).
14. J. Qi, F. Gao, G. Sun, J. C. Yeo, C. T. Lim, HaptGlove–Untethered pneumatic glove for multimode haptic feedback in reality–virtuality continuum. *Adv. Sci.* **10**, 2301044 (2023).

15. B. Zhu *et al.*, Skin-inspired haptic memory arrays with an electrically reconfigurable architecture. *Adv. Mater.* **28**, 1559–1566 (2016).
16. J.-H. Kim *et al.*, A wirelessly programmable, skin-integrated thermo-haptic stimulator system for virtual reality. *Proc. Natl. Acad. Sci. U.S.A.* **121**, e2404007121 (2024).
17. H. Lin *et al.*, *23rd International Conference on Miniaturized Systems for Chemistry and Life Sciences, MicroTAS 2019* (2019).
18. Y. Luo *et al.*, Adaptive tactile interaction transfer via digitally embroidered smart gloves. *Nat. Commun.* **15**, 868 (2024).
19. W. Yang *et al.*, Single body-coupled fiber enables chipless textile electronics. *Science* **384**, 74–81 (2024).
20. Y. Fang, G. Chen, M. Bick, J. J. C. S. R. Chen, Smart textiles for personalized thermoregulation. *Chem. Soc. Rev.* **50**, 9357–9374 (2021).
21. Z. Zhang, Z. J. N. S. R. Bao, High luminescent polymers for stretchable displays. *Nat. Sci. Rev.* **10**, nwac093 (2023).
22. Y. H. Jung *et al.*, A wireless haptic interface for programmable patterns of touch across large areas of the skin. *Nat. Electron.* **5**, 374–385 (2022).
23. Z. Zhang *et al.*, Active mechanical haptics with high-fidelity perceptions for immersive virtual reality. *Nat. Mach. Intell.* **5**, 643–655 (2023).
24. X. Qu *et al.*, Refreshable braille display system based on triboelectric nanogenerator and dielectric elastomer. *Adv. Funct. Mater.* **31**, 2006612 (2021).
25. T. K. Goto, A. W. K. Yeung, J. L. K. Suen, B. S. K. Fong, Y. Ninomiya, High resolution time–intensity recording with synchronized solution delivery system for the human dynamic taste perception. *J. Neurosci. Methods* **245**, 147–155 (2015).
26. J. J. Botha, P. Cannon, J. Hort, Comparing a new rapid combined method (RapCoTT) with traditional approaches for phenotyping thermal taste. *Physiol. Behav.* **238**, 113482 (2021).
27. H. Nakamura, M. Mizukami, K. Aoyama, Method of modifying spatial taste location through multielectrode galvanic taste stimulation. *IEEE Access* **9**, 47603–47614 (2021).
28. N. Ranasinghe, A. Cheok, R. Nakatsu, E. Y.-L. Do, *Proceedings of the 2013 ACM International Workshop on Immersive Media Experiences* (2013), pp. 29–34.
29. N. Ranasinghe *et al.*, Augmented flavours: Modulation of flavour experiences through electric taste augmentation. *Food Res. Int.* **117**, 60–68 (2019).
30. H. Miyashita, *Extended Abstracts of the 2020 CHI Conference on Human Factors in Computing Systems* (2020), pp. 1–6.
31. Y. Zang *et al.*, Influence of olfactory dysfunction on the perception of food. *Eur. Arch. Oto-Rhino-Laryngol.* **276**, 2811–2817 (2019).
32. C. Spence, Factors affecting odour-induced taste enhancement. *Food Qual. Preference* **96**, 104393 (2022).
33. J. B. Phipps, J. R. Gyory, Transdermal ion migration. *Adv. Drug Deliv. Rev.* **9**, 137–176 (1992).
34. I. E. Valkó, H. Sirén, M. L. Riekkola, Characteristics of electroosmotic flow in capillary electrophoresis in water and in organic solvents without added ionic species. *J. Microcolumn Sep.* **11**, 199–208 (1999).
35. R. H. Guy *et al.*, Iontophoresis: Electrorepulsion and electroosmosis. *J. Controlled Release* **64**, 129–132 (2000).
36. V. Dhote, P. Bhatnagar, P. K. Mishra, S. C. Mahajan, D. K. Mishra, Iontophoresis: A potential emergence of a transdermal drug delivery system. *Sci. Pharm.* **80**, 1–28 (2012).
37. K. Ilaslan, I. H. Boyaci, A. Topcu, Rapid analysis of glucose, fructose and sucrose contents of commercial soft drinks using Raman spectroscopy. *Food Control* **48**, 56–61 (2015).
38. K. K. Wang *et al.*, The early, rapid, and non-destructive detection of citrus huanglongbing (HLB) based on microscopic confocal Raman. *Food Anal. Method* **12**, 2500–2508 (2019).
39. Z. Huang *et al.*, Quantitative determination of citric acid in seminal plasma by using Raman spectroscopy. *Appl. Spectrosc.* **67**, 757–760 (2013).
40. X. Huang *et al.*, Garment embedded sweat-activated batteries in wearable electronics for continuous sweat monitoring. *npj Flexible Electron.* **6**, 10 (2022).
41. X. Huang *et al.*, Intelligent soft sweat sensors for the simultaneous healthcare monitoring and safety warning. *Adv. Healthcare Mater.* **12**, 2202846 (2023).
42. G. Plasqui, A. G. Bonomi, K. R. Westerterp, Daily physical activity assessment with accelerometers: New insights and validation studies. *Obesity Rev.* **14**, 451–462 (2013).
43. T. Fark, C. Hummel, A. Hähner, T. Nin, T. Hummel, Characteristics of taste disorders. *Eur. Arch. Oto-Rhino-Laryngol.* **270**, 1855–1860 (2013).
44. M. G. Kang, J. H. Choi, H. S. Kho, Relationships between gustatory function tests. *Oral Dis.* **26**, 830–837 (2020).
45. A. Ikui, A review of objective measures of gustatory function. *Acta Oto-Laryngol.* **122**, 60–68 (2002).
46. Y. Liu *et al.*, Intelligent wearable olfactory interface for latency-free mixed reality and fast olfactory enhancement. *Nat. Commun.* **15**, 4474 (2024).